

## Radiative transfer in 3D model stellar atmospheres

Martin Asplund

*Research School of Astronomy and Astrophysics, Mt Stromlo  
Observatory, Cotter Road, Weston, ACT 2611, Australia*  
(*martin@mso.anu.edu.au*)

Remo Collet

*Institutionen för Astronomi och Rymdfysik, Box 515, SE-751 20  
Uppsala, Sweden (remo@astro.uu.se)*

### Abstract.

Recently 3D hydrodynamical simulations of stellar surface convection have become feasible thanks to advances in computer technology and efficient numerical algorithms. Available observational diagnostics indicate that these models are highly realistic in describing the topology of stellar granulation and for spectral line formation purposes. The traditional free parameters (mixing length parameters, micro- and macroturbulence) always inherent in standard 1D analyses have thus finally become obsolete. These 3D models can therefore both shed light on the elusive nature of stellar convection as well as be employed in element abundance analyses. In the present contribution we will describe some aspects of the models and possible applications of them in terms of radiative transfer.

### 1. Introduction

Reality is (at least) 3-dimensional. This obvious statement is equally applicable to stellar atmospheres, in particular those of late-type stars where the surface convection zone reaches the region responsible for the emitted stellar radiation. Even a casual glimpse of the surface of our own Sun immediately reveals the existence of photospheric inhomogeneities in the form of granulation, in addition to magnetic phenomena like sunspots and flux tubes which probably at some level also are related to the convective motions. Granulation is the direct observational manifestation of convection: concentrated, rapid downdrafts of cool material (intergranular lanes) in the midst of broad, slow upwellings of warm gas (granules). Furthermore, the solar atmosphere is distinctly time-dependent: the individual granules are continuously evolving with typical life-times of a few minutes and waves excited by the convective motions are regularly propagating into the upper layers of the photosphere and the chromosphere. Similar features are expected on other late-type stars and may in fact often be more severe than in the Sun. In view of the dynamic nature of stellar atmospheres, one has to worry whether the use of time-independent hydrostatic 1D model atmospheres as regularly done in for example stellar abundance analyses could lead to severe

systematic errors. Here we will describe efforts currently being made in developing more physically motivated models of stellar atmospheres and the line formation processes, which should hopefully place the findings on firmer footing.

With the advent of supercomputers it is now feasible to perform highly realistic time-dependent 3D hydrodynamical simulations of stellar surface convection (e.g. Nordlund & Dravins 1990; Stein & Nordlund 1998; Asplund et al. 1999, 2000a,b,c; Asplund & García Pérez 2001). Without invoking any of the free parameters traditionally employed in 1D analyses the 3D simulations successfully reproduce a large number of observational constraints such as the granulation topology and detailed line shapes and asymmetries. In this context the energy exchange between the gas and the radiation field is absolutely crucial by largely determining the atmospheric structure and ultimately driving the convection. In the present contribution, special emphasis will be placed on how realistic radiative transfer is achieved both in constructing the 3D convection simulations and in predicting the emergent spectra since different approaches, assumptions and approximations are necessary in the different cases. It is important to emphasize that although the present 3D models are not perfect, the main limitations are of a computational nature, which will be naturally addressed in the future when more powerful computers become available, and due to a lack of manpower. In contrast, 1D models are flawed in a physical sense, since the intrinsic restriction to 1D can not adequately describe all aspects of what is inherently a 3D phenomenon. That is of course not to say that 1D models do not have their merits but it is important to investigate their potential shortcomings, which can only be achieved by comparisons with more sophisticated modelling.

## 2. 3D Hydrodynamical Simulations of Stellar Surface Convection

### 2.1. Ingredients

The 3D hydrodynamical simulations of stellar surface convection described herein have been computed with a 3D, time-dependent, compressible, explicit, radiative-hydrodynamics code (Stein & Nordlund 1998). The hydrodynamical equations for conservation of mass, momentum and energy are solved on a non-staggered Eulerian mesh with gridsizes of  $\approx 100^3$ . The physical dimensions of the grids are sufficiently large to cover many ( $> 10$ ) granules simultaneously in the horizontal direction and many ( $> 10$ ) pressure scale-heights in the vertical. The simulations are thus only covering a small but representative fraction of the whole stellar surface and convection zone, which gives statistically significant results for long time sequences. In terms of continuum optical depth the simulations extend at least up to  $\log \tau_{\text{Ross}} \approx -5$  which for most purposes are sufficient to avoid numerical artifacts of the open upper boundary on spectral line formation which could otherwise skew the results. The lower boundary is located at large depths to ensure that the inflowing gas is isentropic and featureless, while periodic horizontal boundary conditions are employed. The temporal evolution of the simulations cover several convective turn-over time-scales to allow thermal relaxation to be established. The simulations include a hyper-viscosity for stabilization purposes whose parameters are fixed from standard hydrodynamical test cases. No magnetic fields have been included although the code is capable of

simulating magneto-convection. The simulations described here thus only apply to magnetically inactive stars such as the Sun.

Since the intention is to make the simulations as realistic as possible, state-of-the-art input physics is used. The adopted equation-of-state comes from Mihalas et al. (1988), which accounts for ionization, excitation and dissociation of the most important atoms and molecules. The Uppsala opacity package (Gustafsson et al. 1975 with subsequent updates) provide the continuous opacity sources and the extensive lists of Kurucz (1998, private communication) the line opacities. The input parameters characterizing the models are the surface gravity ( $\log g$ ), the overall metallicity ( $[\text{Fe}/\text{H}]$ ) and the entropy at the lower boundary. The effective temperature ( $T_{\text{eff}}$ ) is a consequence of the granulation properties, which depend on the entropy structure. To construct a model with a prespecified  $T_{\text{eff}}$  is therefore a rather time-consuming task involving making several simulations until exactly the right entropy at the bottom has been found which produces the targeted  $T_{\text{eff}}$ . An alternative approach is to settle for a  $T_{\text{eff}}$  in the vicinity of the desired one and carry out a differential analysis with 1D models with exactly the same stellar parameters. This procedure is justified since 3D effects will not change drastically with minor adjustments of the parameters and has been adopted in most cases by us. The reader is referred to Stein & Nordlund (1998), Asplund et al. (1999, 2000a,b) and Asplund & García Pérez (2001) for further details of the 3D convection simulations employed here.

## 2.2. Radiative Transfer

An accurate representation of the energy balance between the gas and the radiation field is crucial in order to achieve a realistic atmospheric structure. We therefore compute detailed 3D radiative transfer at each time-step for a selected number of inclined rays (typically around 10) using a Feautrier-like (1964) long characteristic formal solution. To improve the numerical accuracy, the radiative transfer is solved for a finer depth grid and the results subsequently interpolated back to the original hydrodynamical grid. For computational reasons, the assumption of local thermodynamic equilibrium (LTE) without continuous scattering terms ( $S_{\lambda} = B_{\lambda}$ ) is made throughout. The effects of line-blanketing is accounted for through opacity binning (Nordlund 1982) using normally four opacity bins. The original 2748 wavelength points are sorted into groups representing continuum, weak lines, intermediate strong lines and strong lines. For each bin pseudo-Planck functions are computed and stored in a lookup-table together with the opacities and equation-of-state. Even with the much simplifying assumptions of LTE and only four opacity bins, it is noteworthy that the most time-consuming task in the simulations is the solution of the radiative transfer while the time-integration of the hydrodynamical equations only require a fraction of the time for the highest resolution simulations. We are currently designing methods to switch to a selected opacity sampling technique with 50 – 100 wavelength points instead of opacity binning (Trampedach et al., these proceedings).

## 2.3. Stellar Surface Convection

A recent realisation which has emerged from convection simulations like those described here is the fundamental importance of radiative cooling in a thin

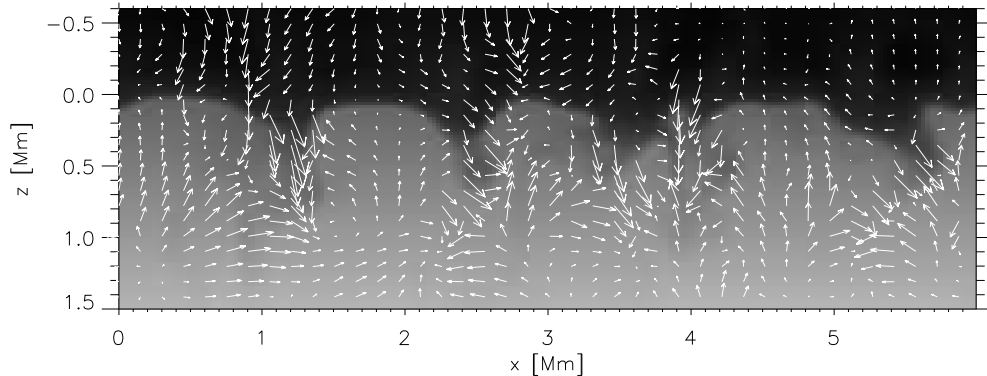


Figure 1. Vertical slice from a 3D solar model atmosphere with the velocity flow field indicated by arrows. The broad warm upflows are characterized by rather slow motion while the cool material is descending relatively rapidly in finger-like structures. Note that the original simulation extends both above and below the region shown here.

surface layer for driving the convection (Stein & Nordlund 1998). As the ascending gas approaches the optical surface radiation starts to escape, lowering the temperature of the gas. In these regions the opacity is very sensitive to the temperature, which means that the opacity decreases rapidly. As a consequence more photons can leak out bringing the temperature down further. This strong feedback causes a sudden drop in the gas temperature, bringing the gas from around 10 000 K to around 5 000 K in about a minute for the Sun. The cooled, entropy-deficient material now has a negative buoyancy and is therefore being accelerated downward. It is noteworthy that almost all buoyancy work is done by the downflows rather than the upflows, which instead are mainly being pushed upwards by mass conservation. This picture is clearly conceptually very different from the traditional view of convection as rising bubbles, as in the mixing length theory or relatives thereof.

Granulation in other solar-type stars is qualitatively similar to the solar case with broad upflows and concentrated downdrafts according to numerical simulations. This is also the case at low metallicities, but there are distinct differences in the optically thin layers. The upflowing gas overshoots into the convectively stable layers above the optical surface. The gas temperature is then determined by a competition between radiative heating and adiabatic cooling due to the expansion following the density stratification. At solar metallicity, the large number of spectral lines (continuum absorption is very inefficient in these optically thin layers) retain the temperature close to the radiative equilibrium value. At low metallicity however, the severe lack of lines shifts the balance towards adiabatic cooling, leading to distinct sub-radiative equilibrium temperatures (Asplund et al. 1999). The temperature difference between a 3D model and a corresponding 1D model can easily reach 1 000 K in the upper layers, which naturally have dramatic consequences for any spectral lines formed in those regions, such as molecular lines.

### 3. 3D LTE Spectral Line Formation

#### 3.1. Radiative Transfer

Using the 3D convection simulations as a time-series of 3D model atmospheres, spectral line formation calculations can be performed which subsequently can be spatially and temporally averaged to produce disk-integrated line profiles. In LTE, the solution of the radiative transfer equation is straightforward as the level populations are directly obtained from the Boltzmann and Saha distributions. This formal solution is computed using a Feautrier (1964) scheme with long characteristics without any continuum scattering terms but accounting for the Doppler shifts caused by the convective motions in the simulations. Before the radiative transfer calculations, the vertical resolution is improved but the horizontal resolution of the original simulation is decreased to typically  $N_x * N_y = 50 * 50$  to ease the computational burden, which however does not encumber the results, as extensive tests show. The calculation of a 3D flux profile require some 100 wavelength points ( $N_\lambda$ ), 10-20 angles ( $N_{\text{angles}}$ ) and at least 50 snapshots ( $N_t$ ) to obtain statistically significant profiles in terms of line asymmetries; for most abundance purposes significantly fewer snapshots are necessary. Thus a single 3D LTE flux profile require typically  $N_t * N_x * N_y * N_{\text{angles}} * N_\lambda \gtrsim 10^8$  1D radiative transfer calculations, which however is still achievable on modern workstations. In addition, the calculations are normally performed for three different element abundances to enable interpolation to the requested line strength. For computational reasons, the monochromatic continuous opacities and equation-of-state data are pretabulated and interpolated during the line calculations. For each snapshot the spatially resolved intensity profiles (Fig. 2) for the different angles are stored, from which a disk-integration can be performed to account for rotational broadening (Dravins & Nordlund 1990) in the final spatially and temporally averaged flux profile. It is important to emphasize that no micro- or macroturbulence enter the calculations.

#### 3.2. Spectral Line Shapes and Asymmetries

The 3D hydrodynamical models described above may be more sophisticated than existing 1D hydrostatic models but they are not necessarily more realistic. Special efforts have therefore been made in comparing in great detail the predictions with observations in terms of for example line shapes and asymmetries to verify how reliable the simulations are. Considering the amazing assortment of strengths, shapes and shifts of spatially resolved profiles, it is obvious that the final averaged profile will be an excellent probe of the atmospheric structure and a very challenging test of the models. Here, the Sun is a perfect test-bench as comparisons can be made without the interference of rotational broadening and information is available for spatially resolved profiles.

As has been well-known since long, 1D models can neither predict the strengths and shapes of lines without invoking the ad-hoc fudge factors micro- and macroturbulence and of course fail utterly to describe line asymmetries. In stark contrast, the 3D line profiles agree almost perfectly with observations, as shown in Figs. 3 and 4 (see also Asplund et al. 2000b, Nissen et al. 2000; Allende Prieto et al. 2002). The self-consistently calculated Doppler shifts arising from the convective motions and to a minor part the oscillatory motions broaden

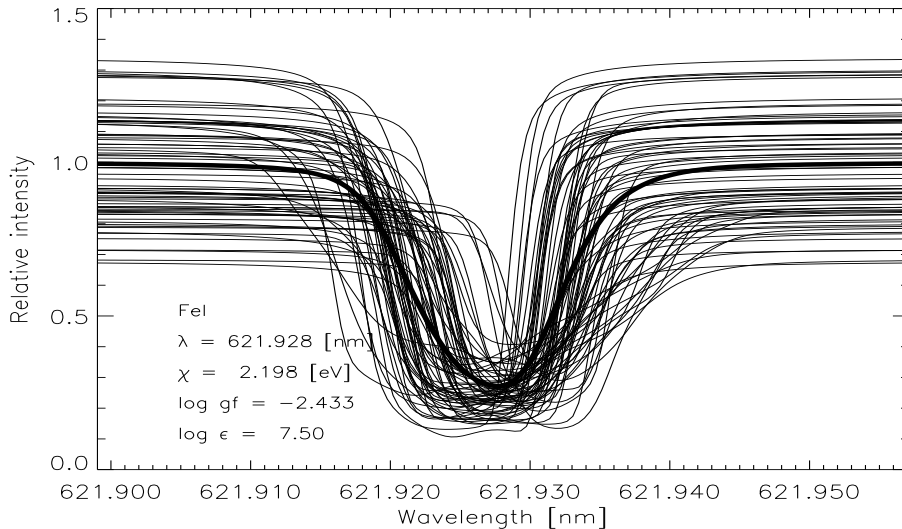


Figure 2. Spatially resolved profiles of the intermediate strong Fe I 621.9 nm line predicted in a 3D solar model atmosphere. Note that the core may occasionally be affected by the artificial upper boundary.

the lines sufficiently. This is also evident from tests when artificially removing all velocity information in the simulations (Fig. 3), giving profiles which closely resemble 1D profiles without micro- and macroturbulence. Thus, the concepts of micro- and macroturbulence introduced in 1D analyses have nothing to do with neither turbulence nor microscopic motions but stems from gradients in the convective velocities which are resolved at the present generation of 3D model atmospheres (Asplund et al. 2000a). This is partly due to the fact that the line formation process is heavily biased towards upflows (large area coverage, high continuum intensity, steep temperature gradients) where the divergent nature of the flow prevents large amount of turbulence to develop in spite of the high Reynolds-numbers of the plasma (Nordlund et al. 1997). The excellent overall agreement between predicted and observed line profiles in general makes it very easy to detect minor blends which otherwise may well have gone unnoticed (Allende Prieto et al. 2001).

Even the detailed asymmetries and shifts of lines are very well reproduced with the 3D simulations, both for the Sun and for other solar-type stars (Asplund et al. 2000b; Allende Prieto et al. 2002), as illustrated in Fig. 4. The accuracy is typically  $0.05 - 0.1 \text{ km s}^{-1}$  for weak lines, which is similar to the uncertainties in the atomic data. In fact, in a few cases the comparisons between predicted and observed solar line profiles have revealed minor typographical errors in tables of laboratory wavelengths. For a large sample of weak solar Fe I lines, Asplund et al. (2000b) found an average difference of  $0.000 \pm 0.053 \text{ km s}^{-1}$  for the observed and theoretical line shifts (with the gravitational redshift removed). Strong lines show a systematic discrepancy in the line core which is likely attributable to effects of the artificial upper boundary or a less realistic temperature structure in the uppermost atmospheric layers. Also the observed behaviour of spatially re-

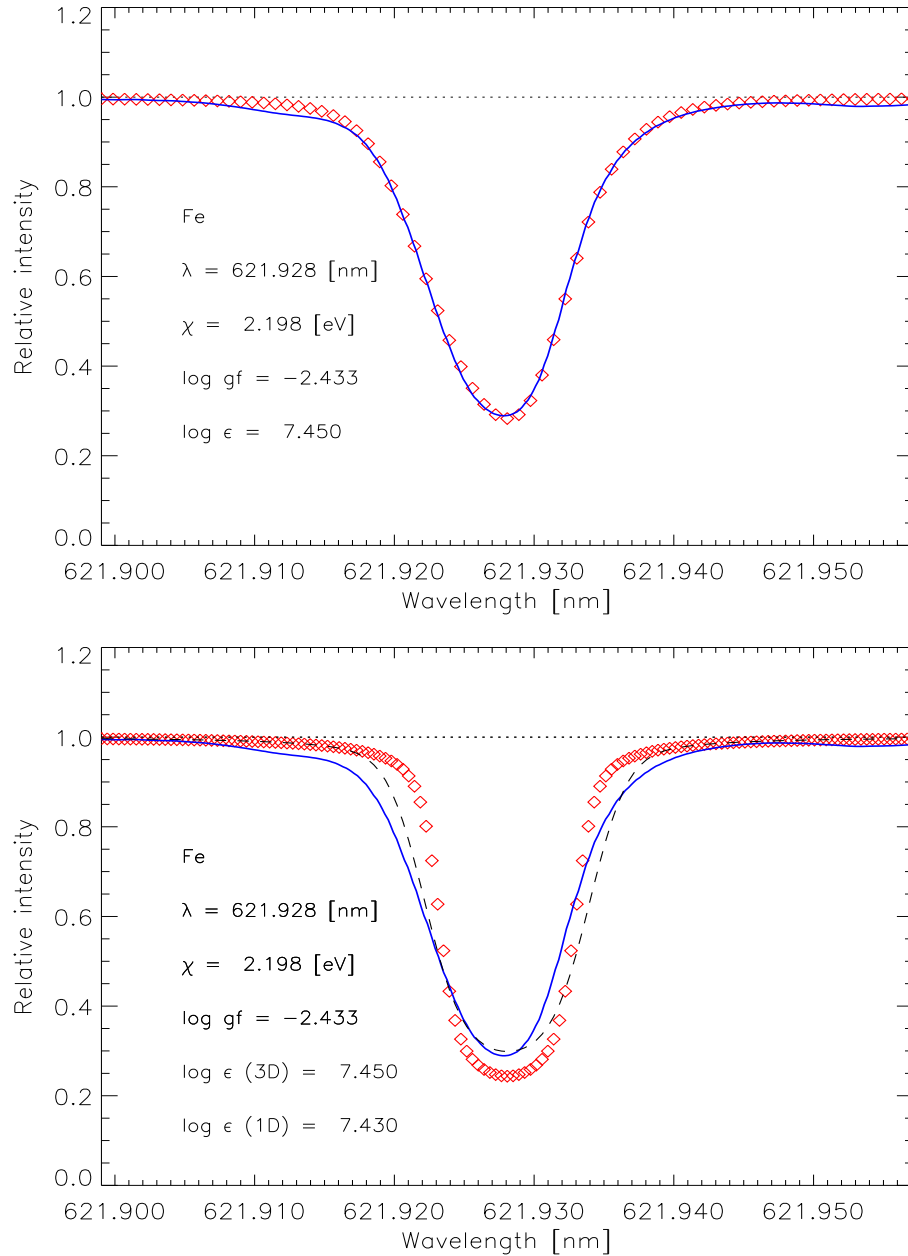


Figure 3. *Upper panel:* Predicted spatially and temporally averaged disk-center intensity profile of the Fe I 621.9 nm line in the Sun (diamonds) compared with observations (solid line). Note the slight problem in the core of this saturated line and the blends in the blue and (far) red wings. *Lower panel:* Same as above but when artificially removing all Doppler shifts arising from the convective motions (diamonds). Also shown is an optimized 1D profile with micro- and (Gaussian) macro-turbulence (dashed line) producing the same line strength as the 3D profile in the upper panel.

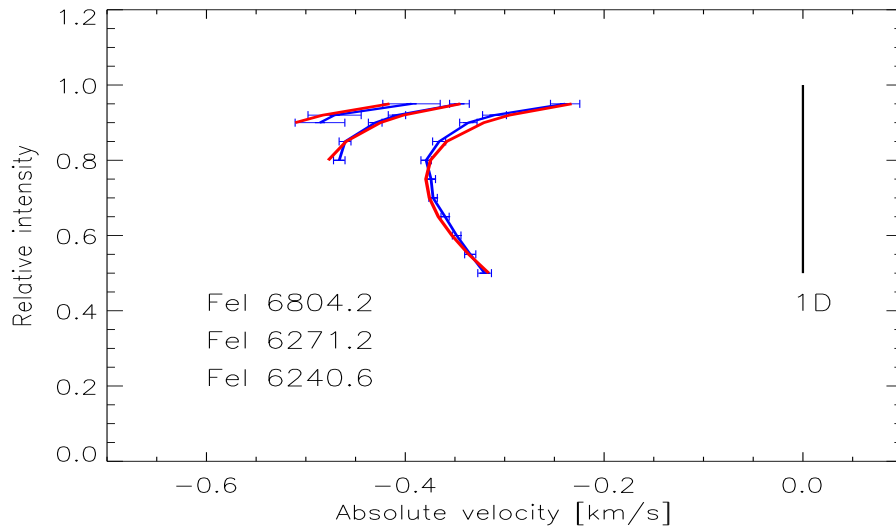


Figure 4. Examples of predicted (solid lines) and observed (solid lines with error bars) spectral line bisectors of a few Fe I lines in the Sun. The agreement even on an absolute wavelength scale is clearly highly satisfactory, while of course the corresponding 1D profiles are purely symmetric.

solved solar line profiles are well matched by the predictions from the simulations (Kiselman & Asplund, in preparation).

## 4. 3D Non-LTE Spectral Line Formation

### 4.1. Radiative Transfer

Line formation does not of course obey LTE in general. To make optimal use of the 3D hydrodynamical model atmospheres described above it is necessary to develop tools that can also handle detailed 3D non-LTE line formation. This challenging task has only recently been addressed with a very promising outlook for the future (Kiselman 1997; Uitenbroek 1998; Botnen & Carlsson 1999; Asplund et al. 2002). The major complication in any non-LTE calculation is of course that the level populations depend on the radiation field which in turn depends on the level populations. The radiative transfer equation must therefore be solved for all relevant wavelengths together with the rate equations of the various levels, normally under the simplifying assumption of time-independence (so-called statistical equilibrium,  $dn_i/dt = 0$ ). To obtain a consistent result, an iterative procedure is adopted using normally an accelerated lambda-iteration technique allowing convergence typically within 10 iterations ( $N_{\text{iter}}$ ). For a normal size model atom there may 100 radiative transitions ( $N_{\text{tran}}$ ), each described with 50-100 wavelengths ( $N_{\lambda}$ ). In total, each 3D non-LTE calculations therefore require  $N_t * N_x * N_y * N_{\text{angles}} * N_{\text{tran}} * N_{\lambda} * N_{\text{iter}}$  corresponding 1D radiative transfer solutions. Hence it should come as no surprise that the formal solution



of the radiative transfer equation with the current estimate of the source function is by far the most dominating task in the calculations. It is not possible to perform such 3D non-LTE calculations for long time-series as can be done in LTE and instead the computations are restricted to a few individual snapshots. Fortunately, 3D non-LTE effects are quite robust entities which differ little from snapshot to snapshot, as verified by various test calculations.

The 3D non-LTE code MULTI3D (Botnen & Carlsson 1999; Asplund et al. 2002) is essentially a 3D version of the widely used MULTI-code for 1D statistical equilibrium calculations (Carlsson 1986). The formal solution of the radiative transfer equation is computed using a short-characteristic method utilizing the horizontal boundary conditions of the 3D atmospheres and accounting for Doppler shifts introduced by the convective motions. The equation-of-state and continuous opacities are provided by the Uppsala package (Gustafsson et al. 1975 and subsequent updates) and allowance for line-blanketing in the photo-ionization rates is possible.

#### 4.2. Li Abundances in Metal-Poor Stars

Given the possibility to estimate the total baryon density of the Universe using the Li abundances in pristine metal-poor halo stars, a large effort has gone into this endeavour ever since the first detection of the Li I 670.8 nm resonance line in such stars (Spite & Spite 1982; Ryan et al. 1999). In view of the large differences in the temperature structures of 3D and 1D models of halo stars (Asplund et al. 1999, see also Sect. 2.3.), there is clearly a great need to study the Li line formation in detail in 3D model atmospheres. Indeed, preliminary calculations assuming LTE indicated that existing 1D analyses had overestimated the primordial Li abundance by as much as 0.2 – 0.35 dex (Asplund et al. 1999). Extreme caution must however be exercised in interpreting these results as Li may be prone to severe over-ionization effects which could compensate the 3D LTE corrections. Indeed our new 3D non-LTE calculations reveal pronounced 3D non-LTE effects which bring the derived Li abundances almost exactly back to those determined with 1D models (Asplund et al. 2002).

With MULTI3D we have recently investigated possible departures from LTE for Li in the two halo stars HD 140283 and HD 84937 using a 21-level Li model atom with 90 radiative transitions (Carlsson et al. 1994). Collisional excitation and ionization due to electrons are accounted for but not the corresponding case of hydrogen collisions, which however have limited impact on the final results. Compared with the LTE case, the Li line is much weaker in non-LTE, as shown in Figs. 5 and 6. In LTE the line is generally strong above the warm upflows while this is not the case in non-LTE, which implies that the population density is largely controlled by the radiation field rather than the local temperature. As anticipated, the main non-LTE mechanism is over-ionization, which decreases the line opacity significantly. In terms of abundances, the 3D non-LTE calculations yield Li abundances well within 0.05 dex to the standard 1D LTE case, at least for these two halo stars. It is noteworthy though that the subordinate 610.4 nm line show an abundance correction of about +0.15 dex compared with 1D, which should be detectable with high enough  $S/N$  observations. It would be premature however from these limited calculations to conclude that the apparent trend in Li abundances with metallicity derived with 1D models (Ryan

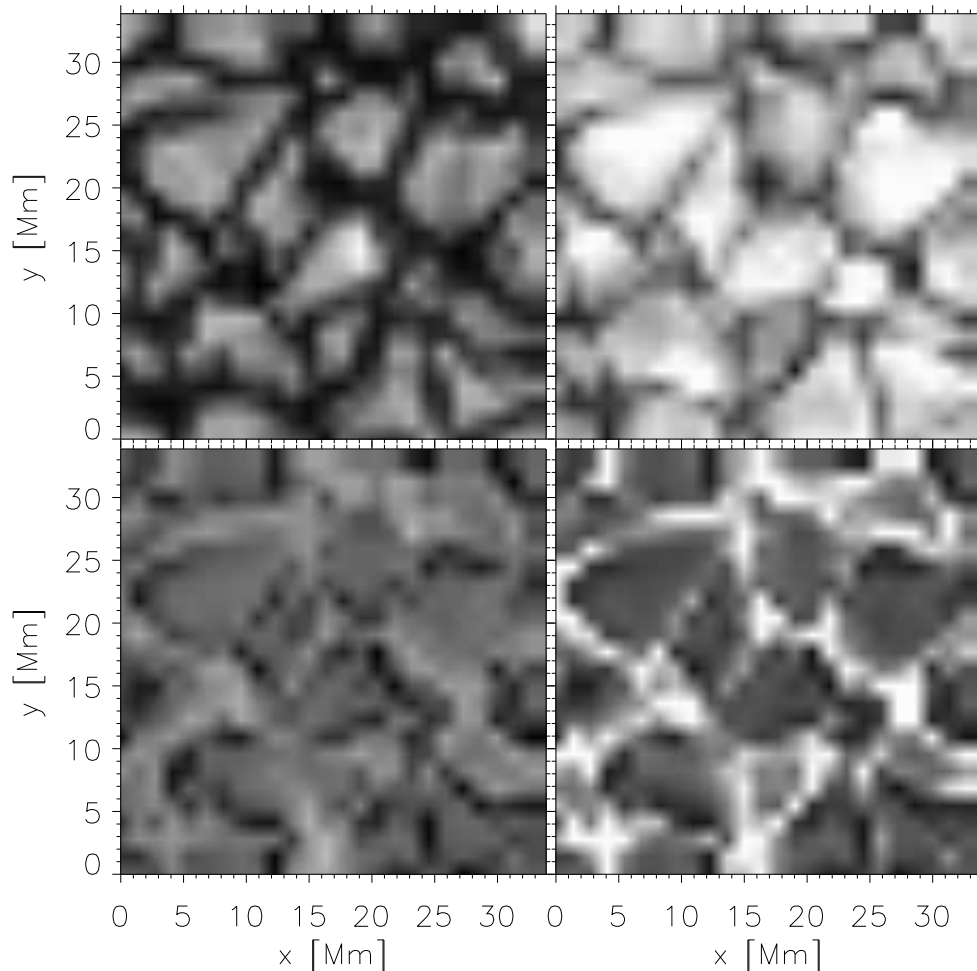


Figure 5. Granulation pattern in HD 140283 seen in disk-center continuum intensity (*upper left panel*) and equivalent width of the Li I 670.8 nm line in LTE (*upper right panel*) and non-LTE (*lower left panel*). Also shown is the ratio of the non-LTE and LTE equivalent widths (*lower right panel*).

et al. 1999) is due to galactic chemical evolution of Li. The exact magnitude of the 3D non-LTE effect will depend on the stellar parameters, in particular  $T_{\text{eff}}$  and  $[\text{Fe}/\text{H}]$ . We are planning to investigate the metallicity dependence of the 3D corrections in the near future.

## 5. Concluding Remarks

With realistic 3D hydrodynamical model atmospheres of late-type stars and corresponding 3D LTE and non-LTE spectral line formation tools now becoming available many potential systematic errors in standard analyses can finally be

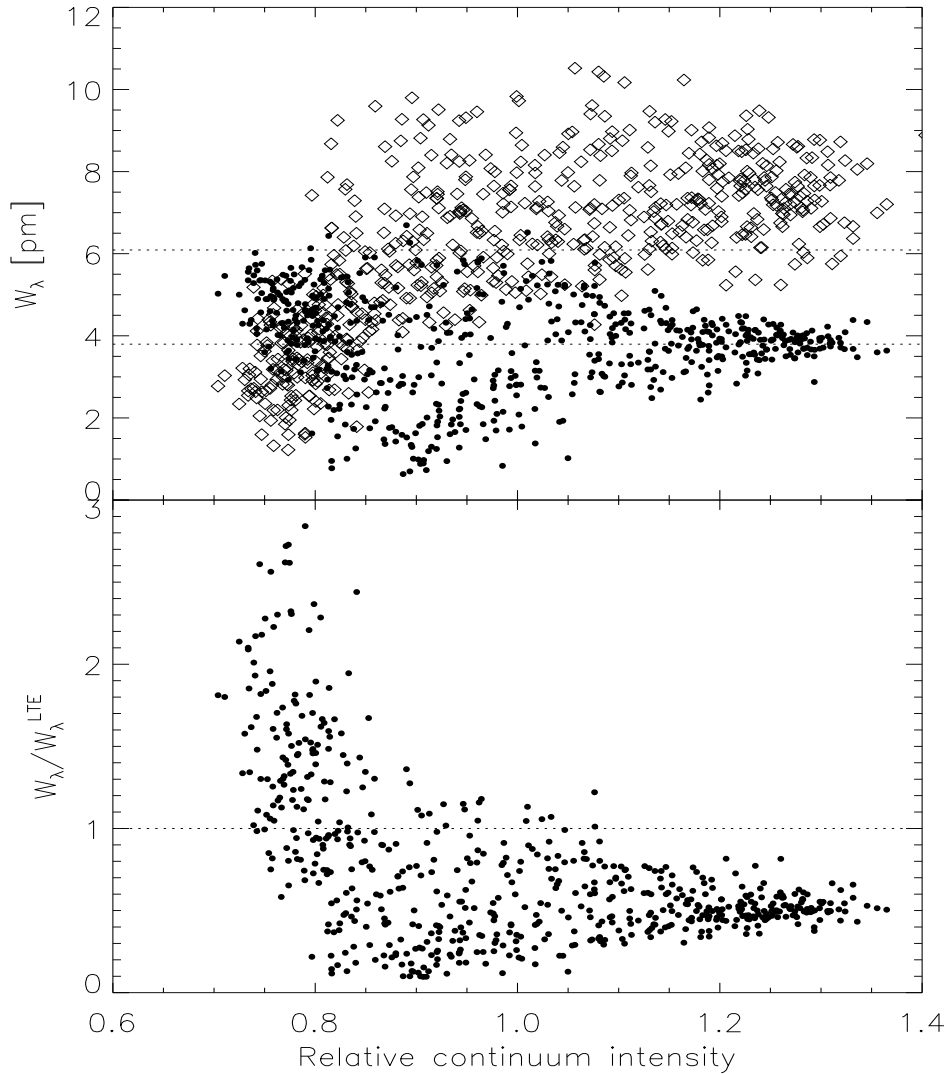


Figure 6. *Upper panel:* Predicted disk-center intensity equivalent widths in HD 140283 in non-LTE (filled circles) and LTE (open diamonds) across the granulation pattern. *Lower panel:* Ratio of non-LTE to LTE equivalent widths.

removed eliminated. In many cases the results may well be dramatically revised (e.g. Asplund & García Pérez 2001; Allende Prieto et al. 2001; Nissen et al. 2002), which can have large impact on the inferred conclusions on stellar, galactic and cosmic evolution. However, the significant efforts in pursuing this ambitious endeavour are justified also for those cases where 3D only confirms previous 1D results as the uncertainties are greatly reduced. The reliability of existing results can clearly only be judged after more sophisticated calculations have been performed.

**Acknowledgments.** We are greatly indebted to the continuing efforts of a large number of wonderful collaborators in the quest of developing 3D model atmospheres and 3D line formation and their applications to astrophysical problems. In particular we would like to mention Carlos Allende Prieto, Mats Carlsson, Ana García Pérez, Nicolas Grevesse, Dan Kiselman, David Lambert, Poul Erik Nissen, Åke Nordlund, Francesca Primas, Jacques Sauval, Bob Stein, and Regner Trampedach. Finally, we are grateful to the editors for their patience.

## References

- Allende Prieto, C., Lambert, D.L., Asplund, M. 2001, *ApJ*, 556, L65  
Allende Prieto, C., Asplund, M., García López, R.J., Lambert, D.L. 2002, *ApJ*, 567, 544  
Asplund, M., García Pérez, A.E. 2001, *A&A*, 372, 601  
Asplund, M., Carlsson, M., Botnen, A.V. 2002, submitted to *A&A*  
Asplund, M., Nordlund, Å., Trampedach, R., Stein, R.F. 1999, *A&A*, 346, L17  
Asplund, M., Ludwig, H.-G., Nordlund, Å., Stein, R.F. 2000a, *A&A*, 359, 669  
Asplund, M., Nordlund, Å., Trampedach, R., et al. 2000b, *A&A*, 359, 729  
Asplund, M., Nordlund, Å., Trampedach, R., Stein, R.F. 2000c, *A&A*, 359, 743  
Botnen, A.V., & Carlsson, M. 1999, in *Numerical astrophysics*, ed. S.M. Miyama et al., 379  
Carlsson, M. 1986, *Uppsala Astronomical Report No. 33*  
Carlsson, M., Rutten, R.J., Bruls, J.H.M.J., & Shchukina, N.G. 1994, *A&A*, 288, 860  
Dravins, D., Nordlund, Å. 1990, *A&A*, 228, 203  
Feautrier, P. 1964, *C. R. Acad. Sci. Paris*, 258, 3189  
Gustafsson, B., Bell, R.A., Eriksson, K., Nordlund, Å. 1975, *A&A*, 42, 407  
Kiselman, D. 1997, *ApJ*, 489, L107  
Mihalas, D., Däppen, W., Hummer, D.G. 1988, *ApJ*, 331, 815  
Nissen, P.E., Asplund, M., Hill, V., D’Odorico, S. 2000, *A&A*, 357, L49  
Nissen, P.E., Primas, F., Asplund, M., Lambert, D.L. 2002, *A&A*, 390, 235  
Nordlund, Å. 1982, *A&A*, 107, 1  
Nordlund, Å., Dravins, D. 1990, *A&A*, 228, 155  
Nordlund, Å., Spruit, H.C., Ludwig, H.-G., Trampedach, R. 1997, *A&A*, 328, 229  
Ryan, S.G., Norris, J.E., & Beers, T.C. 1999, *ApJ*, 523, 65  
Spite, F., & Spite, M. 1982, *A&A*, 115, 357  
Stein, R.F., Nordlund, Å. 1998, *ApJ*, 499, 914  
Uitenbroek, H. 1998, *ApJ*, 498, 427